Effects of Bore-to-Stroke Ratio on the Efficiency and Knock Characteristics in a Single-cylinder GDI Engine

Author, co-author (Do NOT enter this information. It will be pulled from participant tab in MyTechZone)

Affiliation (Do NOT enter this information. It will be pulled from participant tab in MyTechZone)

Abstract

As a result of stringent global regulations on fuel economy and CO2 emissions, the development of high-efficiency SI engines is more urgent now than ever before. Along with advanced techniques in friction reduction, many researchers endeavor to decrease the B/S (bore-to-stroke) ratio from 1.0 (square) to a certain value, which is expected to reduce the heat loss and enhance the burning rate of SI engines. In this study, the effects of B/S ratios were investigated in aspects of efficiency and knock characteristics using a single-cylinder LIVC (late intake valve closing) GDI (gasoline direct injection) engine. Three B/S ratios (0.68, 0.83 and 1.00) were tested under the same mechanical compression ratio of 12:1 and the same displacement volume of 0.5 L. The head tumble ratio was maintained at the same level to solely investigate the effects of geometrical changes caused by variations in the B/S ratio. In addition, because the engine was equipped with a dual CVVT (continuous variable valve timing) system, the valve timings were optimized to fully exploit the potential of each geometry. As a result, lower bore-to-stroke ratios apparently exhibited higher knock resistances not only because of faster burn speeds but also because of the advantage of low unburned gas temperatures under the same valve timing in high-load conditions. However, it was shown that the advantage of a shorter burn duration did not substantially increase as the B/S ratio was decreased below 0.83. Among the tested operating conditions, especially in part load condition, the best efficiency under optimized valve timing was achieved at a B/S ratio of 0.83 because of the paradoxical increase in heat transfer loss observed in lower B/S ratios.

Introduction

Global standards for emission and fuel economy have recently become stringent. For CO2 regulations, the EU targets average emissions from new cars in 2030 to be 30% lower than that of new cars in 2021 according to a legislative proposal from Nov. 2017 [1]. And recently the European council agreed the general approach to set stricter standards (35% lower than 2021's). Along with the recent movement of electrification, increasing the fuel conversion efficiency of internal combustion engines has become more imperative than ever. To satisfy those issues, several studies related to engine efficiency have been investigated, such as fuel and knock characteristics [2], engine turbulence [3], various potential exhaust gas recirculation strategies [4], and valve timing issues [5]. Along with the abovementioned topics, engine geometry should be investigated since it is a very important factor for improving the fuel economy of production engines [6]. Engine geometry includes not only the combustion chamber shape but also other components, such as the injector positions, valve diameters, and intake port design. Among the various parameters, the bore-to-stroke (B/S) ratio of engines is one of the most important parameters affecting the fuel conversion efficiency of SI (spark-ignited) engines.

If the displacement volume and the compression ratio are equal, both the mean piston speed (which is usually related to the turbulence intensity and ignition timing) and the timing at which the flame front touches each component of the combustion chamber can vary depending on the B/S ratio. Most previous studies relating to B/S ratios of SI engines have focused on simulated results [7-11] since it is easy to simultaneously fix both the compression ratio and displacement volume in a simulation. Many of the studies have focused on important parameters, such as turbulence characteristics, heat transfer, and pumping work, induced by various B/S ratios. Only a few studies conducted SI engine experiments for various B/S ratio setups with constant compression ratio and bore [9, 12], which simultaneously produced variations in the stroke and the displacement volume. In general, when the displacement volume increases in the same combustion chamber shape, the overall engine S/V (surface-to-volume) ratio decreases; thus, the cooling loss is expected to be reduced. Consequently, it is difficult to confirm only the correlation between B/S ratio and cooling loss in a situation where displacement volume and compression ratio change at the same time. Thus, an investigation that exclusively focuses on the effects of B/S ratios with a constant compression ratio and a constant displacement volume in SI engine experiments is required, which is the main contribution of this study.

This study is a sequential result of the authors' previous studies [13, 14]. In the first previous work, the author investigated the experimental data using thermodynamic laws and model-based combustion analyses including knock determination methodology. In the second previous work, valve timing variation with various B/S ratios was conducted by using univariate sweep and DoE (design of experiment) process, to find the best efficiency points for each B/S ratio. The focus of this study is to investigate the relationship between thermal efficiency and knock phenomena. In general, several strategies to avoid knock phenomena (e.g., retarding ignition timing) will decrease the amount of work, which causes a deterioration in the net indicated efficiency [15]. Therefore, if certain B/S ratios are more knock-resistive, then they will yield higher efficiency than other B/S ratios, at least in the high-load region. Thus, it is important to investigate the knock characteristics of each B/S ratio to fully exploit the potential of an SI engine.

This paper consists of four chapters. From the next section, the methodologies for the experiments and simulations (1D and 3D) are presented. Additionally, a detailed apparatus for the experiments is

described, and the detailed results and discussions will be followed. Finally, the conclusions of this work will be given in the final part of this work.

Experimental setup

Experimental tests were demonstrated with a single-cylinder GDI engine which is shown in figure 1. This engine was equipped with a dual continuous variable valve timing (dual CVVT) system for both intake and exhaust camshafts. Both camshafts have a longer duration (280 CA for the intake camshaft and 240 CA for the exhaust camshaft) compared to normal camshafts for naturally aspirated engines, which increases the thermal efficiency by utilizing the 'Atkinson' cycle. Intake cam timing can be advanced by 50 CA and the exhaust cam timing can be retarded by 40 CA from their standard valve timing (parking state).

In this study, three B/S ratios (1.0, 0.83 and 0.68) were used. The crank case and cylinder block were shared, whereas each combustion chamber component (cylinder liner and head), piston, connecting rod and crankshaft were used in different B/S ratio setups. Liner thickness was maintained for the similarity of thermal conditions; however, the length of the cooling jacket was inevitably changed. A summary of the specifications is shown in table 1.

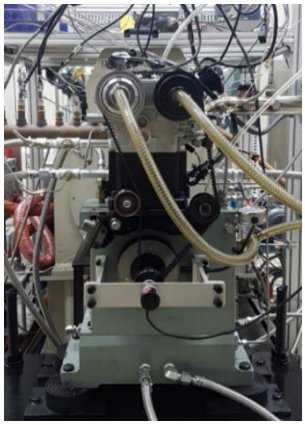

Figure 1. Single cylinder GDI engine with dual CVVT for various B/S ratios

Table 1. Detailed engine specifications.

Type of engine		Single-cylinder Atkinson-cycled dual CVVT		
Compression ratio [-]		12		
Disp. volume [L]		0.5		
Bore-to-Stroke ratio [-]		1.0	0.83	0.68
Stroke [mm]		86	97	111
Bore [mm]		86	81	75.6
Standard Valve Timing (@ 0.1 mm)	EVO	59 CA bBDC		
	EVC	1 CA aTDC		
	IVO	0.5 CA aTDC		
	IVC	100.5 CA aBDC		
Number of valves		4		
Max valve lift		9.5 mm		

Three engines with different B/S ratios had the same displacement volume of 0.5 L while maintaining the same piston top height at TDC (top dead center) position. Therefore, the piston bowl design was slightly changed, from flat surface (B/S ratio of 1.0) to concave surface (2.8 mm bowl height at B/S ratio of 0.68). The compression ratio was maintained at 12 ± 0.1 for all B/S ratios by adjusting the piston bowl (mentioned above) and cylinder head design. Additionally, a shim plate was used by inserting it between the crank case and cylinder block assembly, to compensate the error in mechanical allowance of the compression ratio which was measured by using a swept volume measurement device for all B/S conditions.

In figure 2, a schematic diagram of the engine setup is shown. The AVL Indi-module device and Indicom 2.0 program were used to log the combustion data, including the in-cylinder and manifold pressure signals. A Kistler 6056A piezoelectric in-cylinder pressure transducer was mounted flush in the cylinder head, and the signal was amplified by an AVL IFEM. The Kistler 4045A5 sensor was installed approximately 30 mm ahead of the intake port to measure the intake manifold pressure. Pressure pegging was conducted at BDC (bottom dead center) ± 2 CA during the intake process. A rotary encoder of 3600 teeth (0.1 CA resolution) was used to capture the pressure oscillation by knock with high fidelity. A Horiba MEXA-7100DEGR gas analyzer was used to characterize the emissions, and the air-fuel ratio was monitored by using an ETAS ES631.1 during the engine operation. To control the engine and to acquire the data, an NI cRIO-9039 chassis and a few data acquisition modules were used and the system was run with in-house self-built codes in the laboratory as described in previous studies [13].

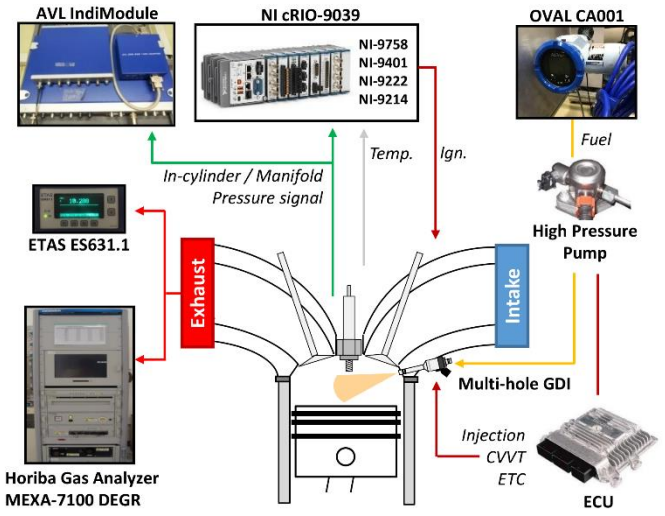

Figure 2. Schematic diagram of the engine experiment

As the difference in the result, such as efficiency and knock propensity, is very small and sensitive to the environment, highly precise experimental methodologies were required for this study. For the measurement of the fuel flow, an OVAL CA001 Coriolis fuel flow meter was used, and the results of the three-minute operation were averaged. The intake air and test cell ambient temperatures were controlled by an air conditioning system, and the oil temperature was also maintained by a controller. As a result, less than 0.5% of the ISFC discrepancy was achieved mainly attributed by a low daily deviation. Conventional gasoline fuel was used of the experiment, and the detailed specifications of the fuel are shown in table 2.

Table 2. Fuel properties

Conventional gasoline	Value	Test Method
H/C ratio	2.064	ASTM D 5291
Density [kg/m^3] @ 15°C	724.5	ASTM D 1298
Research Octane Number	91.5	ASTM D 2699
LHV [MJ/kg]	42.825	ASTM D 240-14
Oxygen [mass %]	1.53	ASTM D 4815
Methanol [mass %]	< 0.05	ASTM D 4815

Methodologies

Knock detection

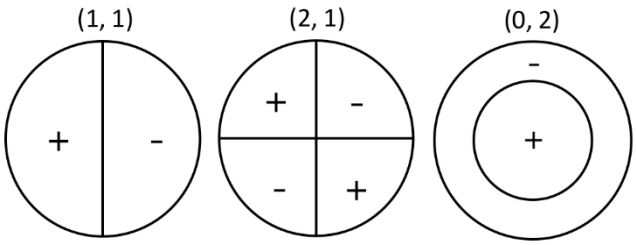

Figure 3. Schematic diagram of oscillation modes (λ, m)

The knock oscillation frequency can vary in different chamber shapes. The general modes are shown in figure 3, and the calculation results of oscillation theory (expressed in equation 1) are shown in table 1. An explanation of the detailed parameters is well described in previous studies [13, 16, 17].

$$f = \frac{\bar{a}}{2\pi} \cdot \sqrt{\left(\frac{\mu^*_{\lambda m}}{B/2}\right)^2 + \left(\frac{\pi g}{Z_0}\right)^2} \quad [Hz] \tag{1}$$

Table 3. Theoretical frequencies of the pressure oscillation modes under three B/S ratios

Oscillation mode (λ, m)	1st (1,1)	2nd (2,2)	3rd (0,2)
$\mu^*_{\lambda m}$	1.841	3.054	3.832
Freq. @ B/S 1.0 [kHz]	6.58	10.92	13.70
Freq. @ B/S 0.83 [kHz]	6.99	11.59	14.54
Freq. @ B/S 0.68 [kHz]	7.49	12.42	15.58

Figure 4 shows the normalized power spectral densities in each B/S ratio, which was derived from experimental data of knocking combustion. As is easily noticed, a lower bore shape leads to a higher knock frequency. From these results, it is thought that incorrect signal filtering may cause unexpected attenuation of the knocking signal. Therefore, instead of conventional bandpass filtering, high-pass filtering using the 9-point median filter method was introduced in this study, as shown in equations 2 and 3. If the absolute maximum pressure value of the filtered signal exceeded the 0.5 bar threshold, the cycle was judged as a knocking cycle. With this TVE (threshold value exceeded) method, MAPO (maximum amplitude of pressure oscillation) incidence (shown in equation 3) was calculated for 1,000 cycles as previously introduced [13], and the knock limit condition was set as the MAPO incidence reached 10%.

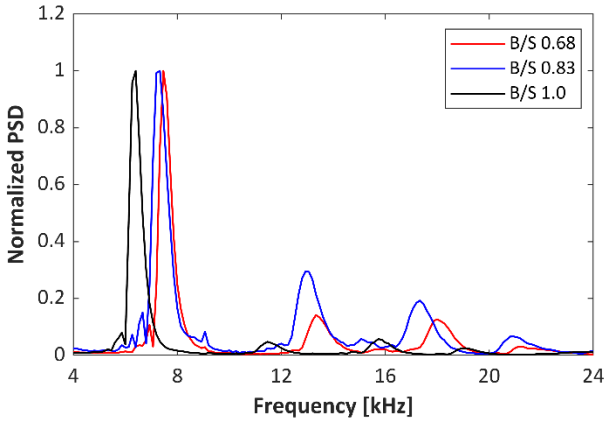

Figure 4. Normalized power spectral densities of the knock signals

$$P_{med,n} = (P_{n-4} + P_{n-3} + \cdots + P_{n+3} + P_{n+4})/9 \tag{2}$$

$$P_{filt} = P - P_{med}, \qquad |P_{filt}| > 0.5\ bar \tag{3}$$

$$MAPO\ Incidence = \frac{N_{knock}}{N_{total}} \times 100 \quad [\%] \tag{3}$$

In summary, KLSA (knock limit spark advance) was determined as the ignition timing when the MAPO incidence reached 10% (of a total number of 1,000 cycles), whereas knock occurrence was judged if the absolute value of the 9-point median high-pass filtered pressure exceeded 0.5 bar.

Experimental methodologies and operating conditions

For determination of the best efficiency point, it was necessary to conduct several processes. In a previous study [14], two processes—univariate analysis and DoE—were conducted. First, a univariate analysis was conducted by changing the intake and exhaust valve timing independently to find the best efficiency point under non-knocking conditions. Figure 5 shows the sensitivity of the ITE (indicated thermal efficiency), which is defined as the difference between the ITE value and the maximum value of ITE for a certain sweep experiment. Each sweep experiment was conducted with other variables fixed; for example, in figure 5, a univariate sweep of the intake valve timing was conducted with a fully retarded exhaust valve timing. Accordingly, it may include some inaccuracies caused by the interaction between the intake and exhaust valve timing, which necessitate a DoE process. As a result, the DoE process was conducted to verify this process. To completely verify the best efficiency point for each actual load condition, the entire valve timing

map was explored as a preliminary experiment to this study; the results are summarized as a contour map, which is shown in figure 6.

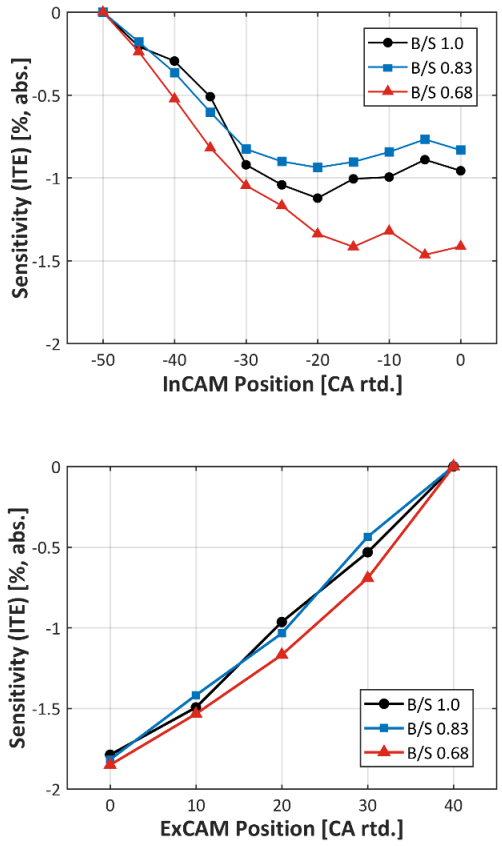

Figure 5. The sensitivity of the net ITE with various exhaust valve timings and B/S ratios (nIMEP 4.5 bar, 2000 rpm): top: figure 5-(a); bottom: figure 5-(b)

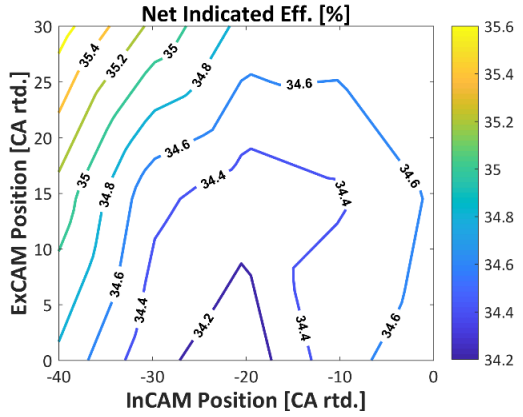

Figure 6. Contour map of the net indicated efficiency at a B/S ratio of 0.68 for various intake and exhaust valve timings (nIMEP 4.5 bar, 2000 rpm)

Regarding the structure of the CVVT, the opening and closing timings shift simultaneously while maintaining their durations. To increase the efficiency while maintaining the same load (nIMEP 4.5 bar) in this process, it is necessary to reduce the efficiency loss associated with gas exchange phenomena such as pumping loss. In the case of exhaust valve timing in the low-load region, it is necessary to strategically retard the EVO (exhaust valve opening) because there is no remarkable loss in blowdown by the decreased amount of air and fuel mixture. Moreover, it is necessary to increase the valve overlap by retarding the EVC (exhaust valve closing) timing to obtain a greater amount of residual gas, which increases the mean pressure during the intake stroke and reduces pumping losses. Therefore, regardless of the B/S ratio, efficiency is always better when the exhaust valve is fully retarded in the low-load region, which was mentioned in our previous work [14], and also shown in figure 5-(b).

For intake valve timing, both fully retarded and fully advanced conditions can increase efficiency. First, for fully retarded IVC (intake valve closing) timing, the intake valve closes (approximately 110 CA aBDC) long after conventional IVC timing due to the LIVC camshaft ('Atkinson' cycle) used in this study. As the effective compression ratio decreases, to achieve the same load with the LIVC camshaft, it is necessary to increase the intake manifold pressure by adjusting the throttle, which results in a reduced pumping loss. However, because of the large amount of backflow from BDC to IVC, a relatively high cyclic variation occurs due to different thermodynamic properties of the mixture, such as the temperature and mixture composition, especially in low load condition. In contrast, with fully advanced IVC timing, RGF (the residual gas fraction) increases as a consequence of valve overlap increase. To achieve the same load with a higher RGF, a less throttling is required, which also results in a reduction in pumping losses. In addition, as RGF is increased, the peak temperature is decreased, which reduces cooling loss during the combustion process (see NOx trends in figures 7 and 9 of previous study [14]). Because of these reasons, intake valve timing with fully advanced shows the best efficiency, regardless of B/S condition, shown in figure 5-(a). Therefore, for the condition with low load (around nIMEP 4.5bar), fully retarded exhaust valve timing and fully advanced intake valve timing were chosen as the best efficiency point where the reciprocal effect was found to be small, investigated by full factorial experiment shown in figure 6.

Table 4. Engine test conditions

Operating condition	Low-load (knock-free)	High-load (knock-related)
Load [bar of nIMEP]	4.5/6.5 ± 0.01	Variable
Fuel rate [mg/cycle]	Variable	26 ± 0.01
Valve timing (IN/EX) [CA rtd.]	-50/40 (optimized)	-35/5
Ignition timing	MBT ± 0.5 CA	KLSA
Injection pressure [bar]	60	100
Injection timing [CA bTDC]	315	
Engine speed [rpm]	1500, 2000	
Lubricant oil temperature [°C]	80 ± 2	
Coolant temperature [°C]	85 ± 1	
Ambient temperature [°C]	26 ± 1	

Table 4 shows the detailed operating conditions of the engine experiments used in this study. Two conditions were investigated. First, part load conditions were used to analyze the characteristics of low-load operation for each B/S condition with the valve timing condition mentioned above. Second, the high-load condition where the fuel rate was maintained at 26 mg per cycle (load was considered as variable) was used to analyze the knock characteristics, which has different valve timing from that of low-load condition. Because of the large amount of fuel (compared to general N/A operation), intake valve was moderately advanced to secure the enough air for stoichiometric operation, while preventing severe knock under fully advanced operation simultaneously. In addition, exhaust valve was advanced for small valve overlap which can make little amount of hot residual gas to prevent knock occurrence.

Simulations (1D and 3D)

Different combustion chamber geometries followed by changes in B/S ratios inevitably accompany not only changes in the in-cylinder flow but also changes in the thermal boundary conditions. For instance, because the heat transfer amount changes, the wall temperatures will be different in spite of the same load condition. Changes in heat transfer amount also includes; the effect of in-cylinder flow which changes convective heat transfer, combustion efficiency and phasing. Furthermore, the conductive heat transfer between components such as cylinder head and liner also varies due to changes in geometry. This change is a very complex phenomenon, which is almost impossible to control all the parameters to identify or separate each effect. Therefore, in this study, 1D simulation was adapted to roughly understand the experimental results.

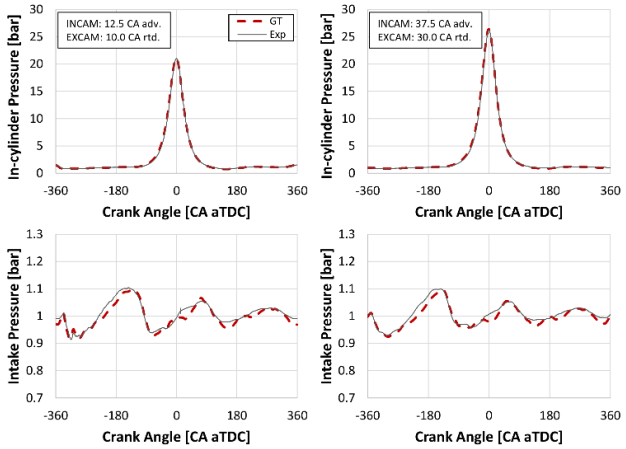

Figure 7. Motoring simulation results at B/S ratio of 1.0, 2000 rpm

As the reliability of the experimental test results was verified, 1D engine model including a wall temperature solver was established using GT-power. Based on the motoring pressure data, the shapes of the air exchange paths were optimized to imitate all the in-cylinder and manifold pressures in various conditions, such as different engine speeds, valve timing and intake pressures. Imitation of flow characteristics is very important as it significantly affects the variation of RGF, especially in Atkinson-cycled engine with LIVC in this study. Figures 7 shows the examples of the matched results. Figure 7 includes the small and large valve overlap case at 2000 rpm and a B/S ratio of 1.0. To prevent complexity, the result was only shown for two valve overlaps in a B/S ratio of 1.0; however, the model was validated in a wide range of parameters, including engine speed, wall temperatures (cold/hot), valve timing, and even B/S ratios. In the figures, the black line indicates the experimental result, and the red line indicates the simulated data. Due to the long duration cam for LIVC, advancing the IVC results in a higher peak pressure, which means that the effective compression ratio was increased. It is apparent that the established model considerably imitates the characteristics of the actual engine, including the pressure fluctuation.

After the flow characteristics were reproduced by the model, combustion data were also matched at each KLSA condition under different B/S ratios based on experimental results. Due to the incompleteness of conventional models of heat transfer, combustion and flow, it is almost impossible to imitate all the experimental results using the simulation. Therefore, as the objective of 1D simulation of this study is to extract the RGF values and thermal boundary conditions, the coefficients of models were optimized based on minimization of the discrepancy of in-cylinder pressures between simulation and experiment.

For the combustion model, to simply match the experimental data, the ‘Wiebe’ function was used with coefficient tuning. The burn duration and anchor angle (CA50) of Wiebe function could be extracted from the 0D combustion analysis of experimental result. However, due to the difference in mechanisms between 1D simulation and 0D analysis, those values were biased for all conditions using optimization during the combustion period. Subsequently, Wiebe exponent and Woschni multiplier were optimized to minimize SSE (sum of squared error) between simulated pressure and experimental pressure data from SOC (start of combustion) to EOC (end of combustion). The ‘TwallSoln’ function was adapted to calculate the thermal interactions between components as well as the heat transfer. This whole process was iteratively conducted in every single case to characterize the steady-state operation.

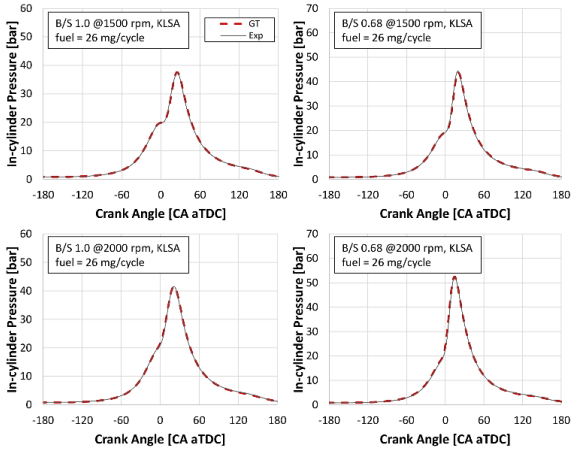

Figure 8. Firing simulation at KLSA, m_f = 26 mg/cycle at B/S ratios of 1.0 and 0.68

Figure 8 shows the GT-power simulation results of firing conditions at 1500 and 2000 rpm and B/S ratios of 1.0 and 0.68. A splendid agreement was achieved, and this result provided the thermal boundary conditions for the 3D CFD (computational fluid dynamics) simulation and an estimated value of the RGF under each experimental condition. However, because the test was conducted at KLSA condition under each B/S ratio and engine speed, it is difficult to conclude that the change in the thermal boundary condition was

attributed to the B/S change because the operating parameters in each condition are different.

An example of the piston surface temperatures at 2000 rpm and KLSA condition is shown in figure 9. The piston surface temperature is determined by complex behavior, including convective heat transfer from the in-cylinder gas, ring and skirt friction, and the piston shape and material. Because thermal boundary conditions are sensitive to operating conditions, although it is steady-state operation, error in the results still exist. Therefore, to minimize the error, the thermal properties of components were tuned by validation with actual measurement data of temperatures [18].

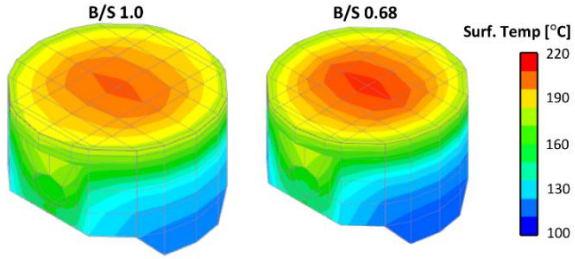

Figure 9. Estimation of the piston surface temperature using 1D simulation (GT-power) at KLSA, 2000 rpm, and B/S ratios of 1.0 and 0.68

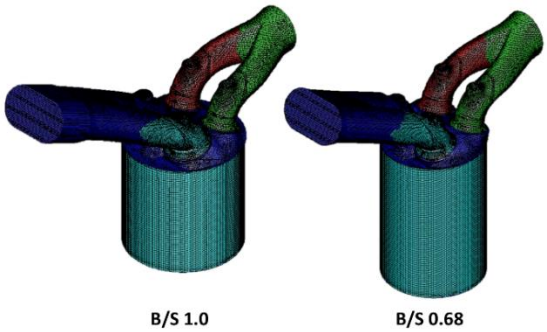

Figure 10. Engine mesh generated at BDC for B/S ratios of 1.0 and 0.68

In this study, 3D CFD simulation was conducted based on confirmed valve timing by the 1D simulation results. In addition, thermal boundary conditions were obtained from the 1D simulation results as previously described. STAR-CD V4.24 was used as a simulation tool, and the mesh number of the engine model was approximately one million at BDC. The 'Angelberger' function was used for the heat transfer calculation, and the k-ε-RNG model was used to simulate turbulence. Figure 10 shows the mesh designs of two B/S ratios: 1.0 and 0.68.

Results and discussion

Figure 11 shows the results of nITE (net indicated thermal efficiency) for three B/S conditions at six different conditions – nIMEP (net indicated mean effective pressure) 4.5 bar, 6.5 bar, and fuel rate of 26 mg/cycle in 1500 and 2000 rpm. nMEP 4.5 bar was non-knocking condition for all B/S ratios, however, B/S ratio of 1.0 showed slightly knocking behaviors at nMEP 6.5 bar in conditions of both 1500 and 2000 rpm.

In part load condition, it was shown that the advantage of decrement in surface area was decreased as the B/S ratio decreased below 0.83. In all cases, the efficiency was increased as the load increased, and it is mainly attributed to reduction of fractions of pumping loss and cooling. However, different behaviors were shown in 26 mg/cycle cases due to the retarded spark timing by knock constraints for all B/S ratios. Under knocking condition, B/S ratio of 0.68 showed the best efficiency.

This might be somewhat different conclusion from previous studies. As previously described, investigation on B/S ratio were generally conducted increasing stroke while the bore size was maintained. Therefore, in this study, the compression ratio and the displacement volume were fixed. As a result, it was found that the decrease of B/S ratio is not always a promising method for increasing the efficiency.

Following sections consist of different two parts: part load condition and knocking condition, as the effect of B/S ratio was distinctively different.

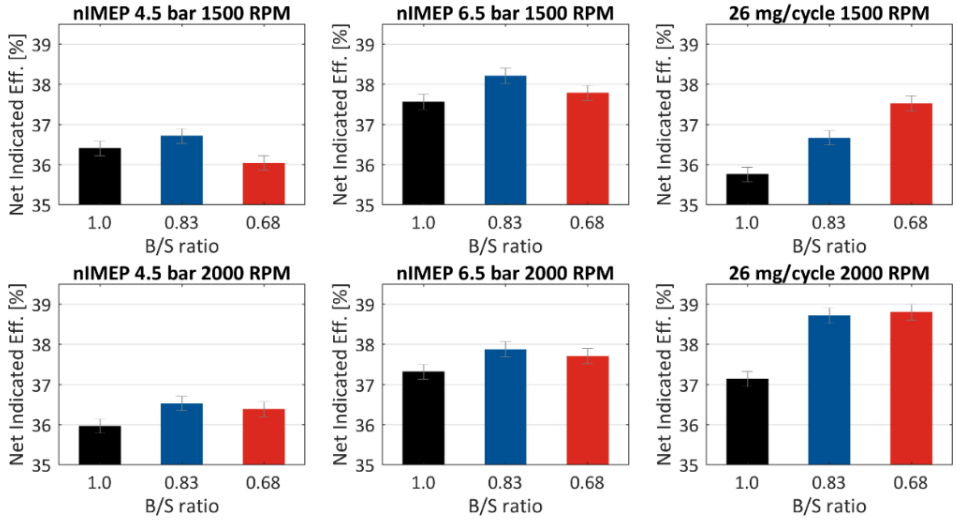

Figure 11. Net indicated thermal efficiencies at different loads (nIMEP 4.5, 6.5 bar and m_f = 26 mg/cycle) and speeds (1500 and 2000 rpm)

Part load condition

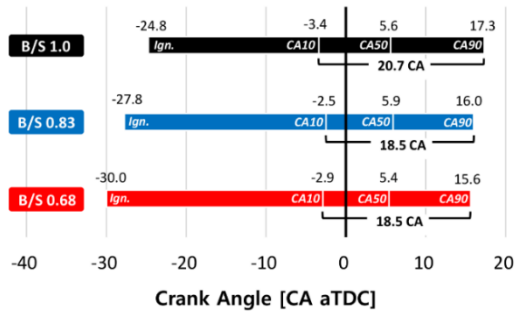

Figure 12. Combustion parameters at nIMEP 4.5 bar, 2000 rpm.

The combustion phasing parameters such as ignition timings and burn durations (CA10 – CA90) at nIMEP 4.5 bar and 2000 rpm are illustrated in figure 12. It should be noticed that a further decrease of burn duration was not achieved as the B/S ratio decreased below B/S ratio of 0.83. This also elucidates the efficiency enhancement by combustion improvement was saturated at near B/S ratio of 0.83 in part load condition. In addition, to maintain the MBT (maximum brake torque) timing, at which the CA50 was between 5-6 CA aTDC, B/S ratio of 1.0 showed the most retarded ignition timing (24.8 CA bTDC) than those of other two B/S ratios; 27.8 CA bTDC at B/S ratio of 0.83 and 30 CA bTDC at B/S ratio of 0.68. This implies that the initial flame growth and speed is faster in B/S ratio of 1.0 ironically, while it is generally thought that lower B/S ratio increases the in-cylinder turbulent intensity.

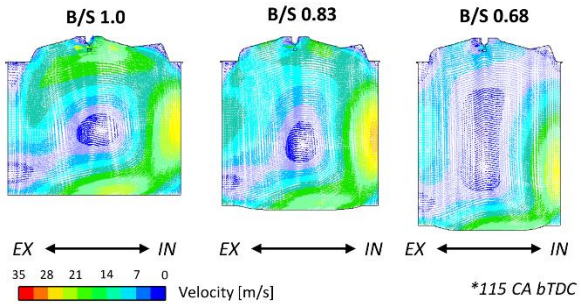

Figure 13. Flow motion during intake process at nIMEP 4.5 bar, 2000 rpm

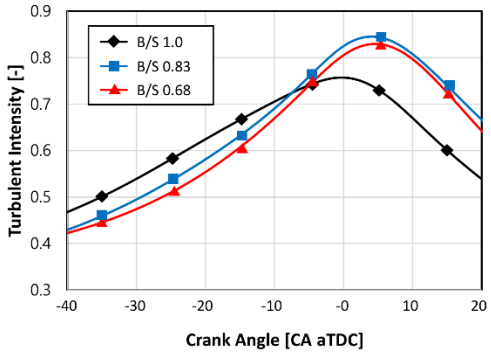

Figure 14. Turbulent intensity at 4.5 bar, 2000 rpm (motoring)

Figures 13 and 14 show the 3D CFD simulation results of in-cylinder flow velocity and turbulent intensity, respectively. The simulation was conducted in motoring condition with intake pressures based on experimental data. In figure 13, the flow velocities at 115 CA bTDC and 2000 rpm are shown. As it is easily noticed, B/S ratio of 0.68 shows the lowest flow velocities near top head surface and near the spark plug, and the velocity decreases as the B/S ratio decreased. This result elucidates the reason why ignition timing had to be advanced with B/S ratio decrease to maintain MBT timing. In addition, lower B/S ratio engine showed a stretched and weak tumble motion due to the rectangular shape of the cross-sectional plane.

Figure 14 illustrates the in-cylinder averaged turbulent intensities. Based on the experimental result, the ignition timing was located between 20 – 30 CA bTDC to achieve the MBT timing, the turbulent intensity was shown as the highest at B/S ratio of 1.0 and the lowest at B/S ratio of 0.68. The turbulent intensities in B/S ratios of 0.86 and 0.68 increased rapidly until the end of compression which contributed to the shorter burn durations during the combustion. However, no significant advantage was found in B/S ratio of 0.68 compared to 0.83, and this also interprets that the effect of efficiency increase was saturated near B/S ratio of 0.86.

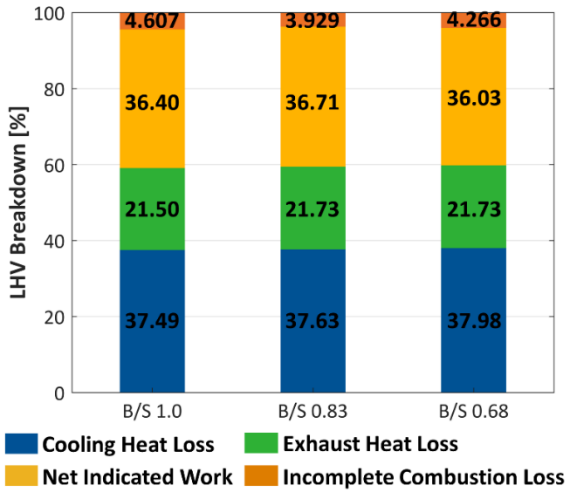

Figure 15. Percent fuel heating value at nIMEP 4.5 bar, 1500 rpm (reproduced from [14])

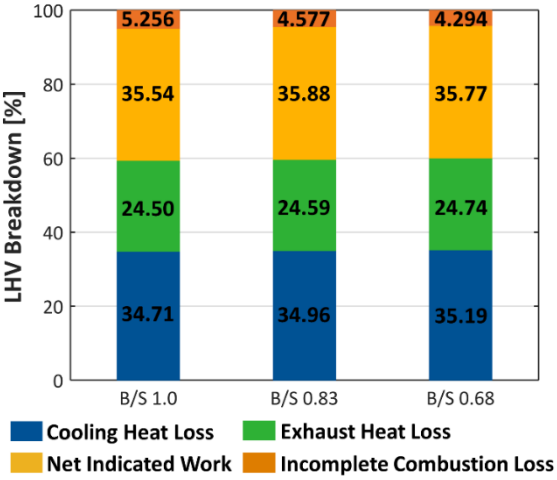

Figure 16. Percent fuel heating value at nIMEP 4.5 bar, 2000 rpm

The results of energy balance in low-load operations (nIMEP 4.5 bar) are plotted in figures 15 and 16 (including 1500 rpm case reproduced from previous study [14]). The details to calculate each component of energy distribution (e.g. cooling heat loss, incomplete combustion loss) were referred from a previous study [19]. In all cases, cooling loss accounts for over 30% which is relatively higher than conventional production engines due to the characteristics of single-cylinder engine. In addition, for both 1500 rpm and 2000 rpm conditions, incomplete combustion loss was higher in B/S ratio of 1.0 than those of other lower B/S ratios, and this is attributed to the increased crevice volume. In the previous study [14], it was suggested that the unexpected behavior was originated from the increased heat transfer which might increase the cooling loss when B/S ratio decreased; thus, the advantage of heat loss reduction by the decrease in S/V (surface-to-volume) ratio, was diminished in lower B/S ratios. In this study, the same tendencies were observed in the nIMEP 4.5 bar and 2000 rpm condition as shown in figure 16, wherein increase in cooling loss was also observed as B/S ratio was decreased.

Another issue that deserves detailed investigation is the tendency of exhaust heat loss. Fundamentally, this heat loss is strongly dependent on the exhaust temperature. In general, when the other variables are consistent, the end of combustion timing is significantly related to the exhaust temperature; the faster combustion ends, the lower the exhaust temperature is. For almost all experimental data, including those shown in figures 15 and 16, the burn duration (CA10-90) under a B/S ratio of 0.68 was approximately the same or slightly shorter than that under a B/S ratio of 0.83, whereas the exhaust temperature under a B/S ratio of 0.68 was slightly higher than that under a B/S ratio of 0.83. A further investigation is still required, however, it is expected the work extraction would be deteriorated by several reasons during expansion stroke: the variations in heat transfer under different volume profiles caused by different stroke, bore and connecting rod conditions, etc.

Knocking condition

Considering that the incomplete combustion loss was not significantly different when B/S ratio changed especially for B/S ratios of 0.83 and 0.68, it is reasonable to assume that the mass of the mixture is almost the same under stoichiometric conditions (λ=1) if the fuel input mass is maintained. Therefore, to investigate the effects of different B/S ratios on the knock phenomena, the amount of fuel was maintained at 26 mg/cycle in this section. As the engine was equipped with a long duration LIVC intake camshaft, under naturally aspirated conditions, the intake valve timing had to be advanced to secure enough air intake amount to achieve high-load for knocking combustion. Meanwhile, to decrease the residual gas fraction for knock suppression, exhaust cam shaft was retarded. The operating conditions for the high-load knocking test are also shown in table 4.

Figure 17 shows a KLSA test result of each B/S ratio at 1500 rpm. The pumping work was not significantly different as the B/S ratio changed as shown in the figure. Therefore, the net work was indicated in this study. As previously described, ignition timing advance was conducted until it reached to KLSA. In each B/S case, the leftmost data point indicates the KLSA condition.

As it is easily noticed, the B/S 1.0 condition has the worst knock resistance as the knock incidence already reached the limit when the CA50 was only advanced to 19.9 CA aTDC. The CA50 could be advanced until 15.4 CA aTDC at B/S ratio of 0.83 and until 15.0 CA aTDC at B/S ratio of 0.68. The CA50 at KLSA was not significantly

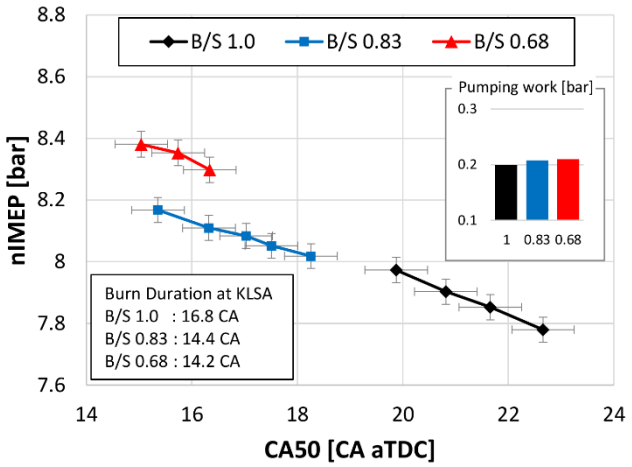

Figure 17. Variation in nIMEP and CA50 at 1500 rpm, m_f=26 mg/cycle, and λ=1

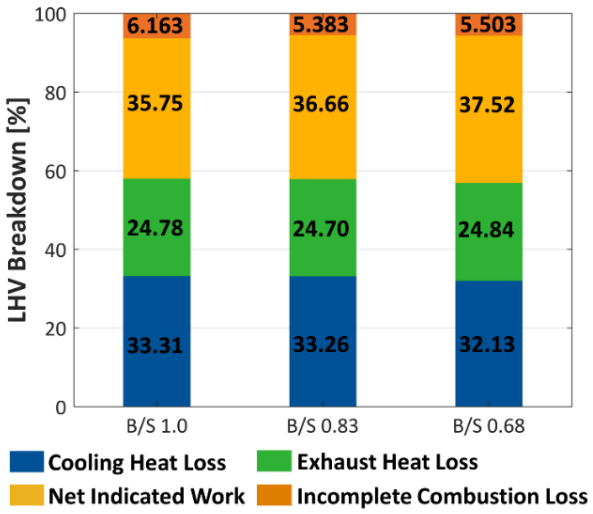

Figure 18. Percent fuel heating value at KLSA, 1500 rpm, m_f=26 mg/cycle, and λ=1

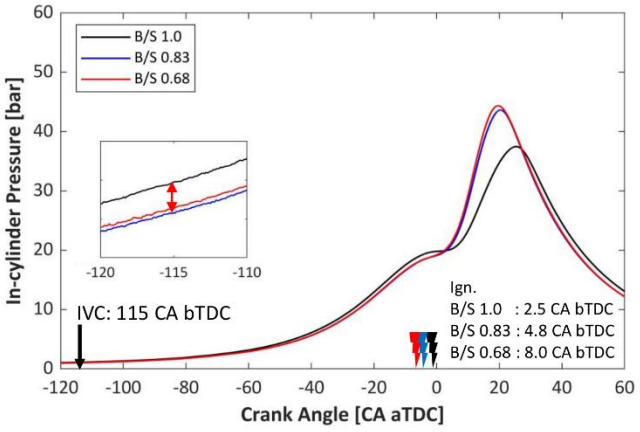

Figure 19. In-cylinder pressure at KLSA, 1500 rpm, m_f=26 mg/cycle, and λ=1

different between B/S ratios of 0.83 and 0.68. In addition, due to similar advances in ignition timing of KLSA, the burn duration was also short enough in at a B/S ratio of 0.83 (14.4 CA) compared to that B/S ratio of 0.68 (14.2 CA).

Figure 18 shows the percent fuel heating value of the 1500 rpm case. It is apparent that the cooling loss was decreased at B/S ratio of 0.68 case. Therefore, it is thought that the achievement of a higher load in the B/S 0.68 condition is attributed to the reduction in cooling loss despite of increase in exhaust loss. Unlike part load condition, it is considered that the reduced surface area of the lower B/S ratio near the firing TDC led to a decrease in cooling loss. This tendency resulted in one noticeable result in figure 18, wherein the collinear line of the B/S 0.68 condition is located above the other two lines.

Figure 19 shows the in-cylinder pressure curves at 1500 rpm and KLSA timing of each B/S ratio. It should be mentioned that the pressure at IVC timing at B/S ratio of 1.0 is obviously higher than at other two B/S ratios. As this test was conducted under constant fuel input amount conditions, the total trapped mass can be considered almost the same. In addition, the valve timing was also maintained the same and the input air temperature was held consistent during the test. The difference in the residual gas fraction was not shown to be significant via the GT-power simulation (9.2%, 9.0% and 8.9% of the total mass fraction was observed). Therefore, it can be suggested that the difference in the pressure value was caused by thermal interactions among the in-cylinder residual gas, fresh mixture and chamber surfaces. This discrepancy might include the differences among the residual gas temperatures under each B/S ratio. In the B/S 1.0 condition, due to a higher pressure, the unburned gas temperature at IVC was higher (approximately 20 K by a simple 0D calculation) than under the other two B/S ratios, which possibly deteriorated the knock resistance by increasing the overall unburned gas temperature and resulted in a retarded KLSA.

Figures 20 to 22 show the results in the 2000 rpm case. The load as a function of CA50 is shown in the figure 20; in the same way as the former result, the leftmost point on each line is the KLSA condition. The overall load was increased in all B/S ratios as the engine speed was increased compared to 1500 rpm case. The best efficiency was also achieved at B/S ratio of 0.68, and the CA50 at KLSA was advanced to 9.7 CA aTDC, whereas it could only be advanced to 11.5 CA aTDC at B/S ratio of 0.83. However, unlike the 1500 rpm case, the B/S 0.83 line is almost collinear with the B/S 0.68 case, which implies that the advantage in reduced cooling loss provided by a decreased surface area of combustion chamber, was not increased by further decreasing the B/S ratio to 0.68 below 0.83. RGF was estimated at 7.9%, 8.66% and 8.62% for B/S ratio of 1.0, 0.86 and 0.68, respectively, which is also not a significant difference.

Two interesting things were noticed. First, overall CA50 timings at KLSA for B/S ratios of 0.83 and 0.68 were advanced to near general MBT timings as shown in the figure 20. Thus, as the in-cylinder temperature was increased in response to the ignition timing advance, the increase in cooling loss began to deteriorate the increase in gross work, i.e., the rate of increase in the load was almost saturated. Second, at the same CA50 timing, B/S ratio of 0.83 had an even higher nIMEP value than that at B/S ratio of 0.68. Theoretically, if the same CA50 corresponds to similar exhaust heat loss trend, the difference in net work (i.e., nIMEP) can be caused by cooling losses. That is, the burn duration under B/S ratio of 0.83 is short enough to exploit the potential of fast combustion in this condition; in B/S ratio of 0.68 condition, increase in fraction of cooling loss was higher than that of in B/S 0.83 condition, this phenomenon was partly observed

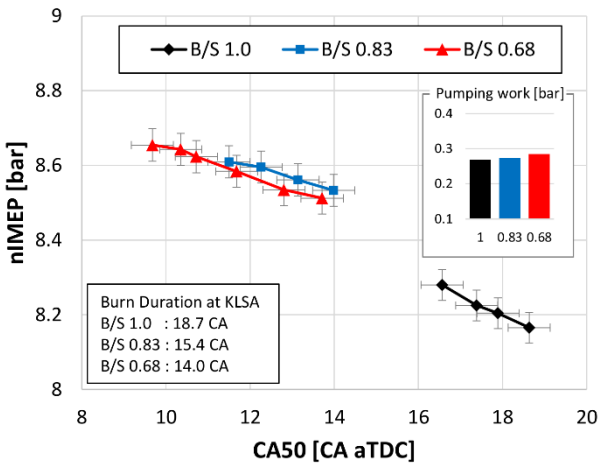

Figure 20. Variations in nIMEP and CA50 at 2000 rpm, m_f=26 mg/cycle, and λ=1

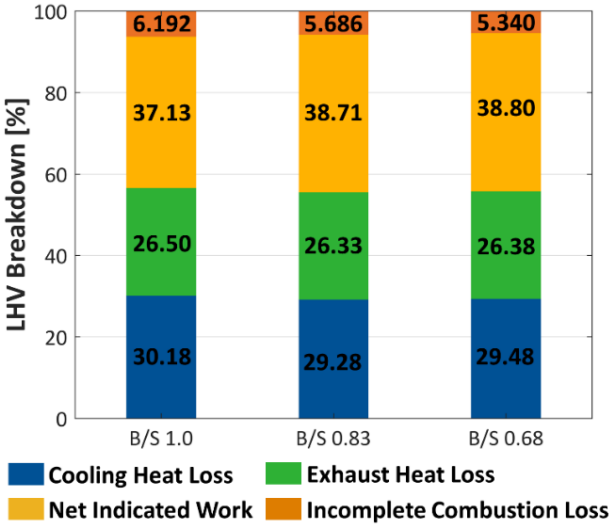

Figure 21. LHV breakdown at KLSA, 2000 rpm, m_f=26 mg/cycle, and λ=1

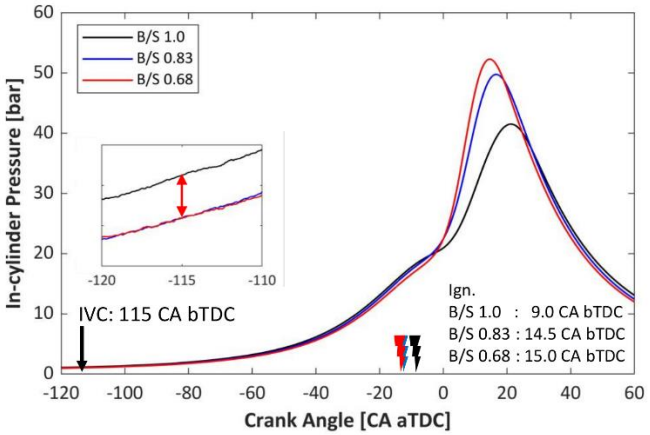

Figure 22. In-cylinder pressure at KLSA, 2000 rpm, m_f=26 mg/cycle, and λ=1

in the part load condition as well.

As the test was conducted under consistent fuel mass input conditions, increased load directly means an increase in efficiency. At the B/S 1.0 condition, the ISFC at KLSA was 226.3 g/kWh and 235.0 g/kWh at 1500 rpm and 2000 rpm, respectively. As the B/S ratio was decreased to 0.83 and 0.68, the ISFC was decreased by 3.7% (217.8 g/kWh) and 4.3% (216.6 g/kWh), respectively, at 1500 rpm. In the 2000 rpm case, a 2.3% (229.6 g/kWh) and 4.9% (223.4 g/kWh) decrease in the ISFC was observed at B/S ratios of 0.83 and 0.68, respectively.

As the gas exchange process is very complex phenomenon, thus it is not able to elucidate completely, however, discrepancies in pressure at IVC timing is mainly attributed to the differences in: thermal property of residual gas, heat transfer between mixture and walls, other impacts such as charge cooling effect of injected fuel. As the differences in exhaust gas temperatures were no significant (within 3K in all conditions) and the injected fuel amount was the same, the investigation focusing on heat transfer process was attempted for deeper understanding in this study. For clarity in this paper, results are only shown for B/S ratios of 1.0 and 0.68, except the 0.83 case.

In figures 23, the total heat transfer amounts from gas to wall are shown from the intake valve opening (IVO) to 70 CA bTDC at 2000 rpm under two B/S ratios of 1.0 and 0.68. The intake pressure profiles were based on the experimental results, and the thermal boundary conditions were extracted from the 1D simulation as previously described. 70 CA bTDC timing (referred as inverse timing) was chosen because, after this timing, the heat flux is reversed by increased gas temperature.

During the gas induction and the early stage of compression stroke, more heat from the wall to gas was transferred in B/S ratio of 1.0 condition, compared to B/S ratio of 0.68 case. The intake port has the largest contribution to increasing the gas temperature among all the components in both conditions, as previously reported [18, 20-22]. Despite the average piston surface temperature was increased in B/S ratio of 0.68 as shown in the figure 10, the role of the piston on increasing mixture temperature was decreased. It is thought that reduction of the surface area and change in the flow motion reduced the total heat transfer.

In figure 24, the reversed heat transfer amounts from gas to wall after the inverse timing are shown. Increased heat transfer amount to the liner wall was observed in lower B/S due to increased liner surface area and reduced wall temperature, while B/S of 1.0 showed the larger amount on that of the piston and head surfaces.

In general, specific heat of the mixture is small in the early stage of compression stroke due to the low temperature, causing high pressure rise rate with same amount of heat. Therefore, despite of small difference in amount of heat during this stage (shown in figure 23), the discrepancy of pressure could be detected at IVC timing between B/S ratio of 1.0 and 0.68. Of course, not only this effect but also aforementioned other factors might lead to the higher pressure at B/S ratio of 1.0. On the other hand, during latter stage of compression stroke after the inverse timing, the mixture was sufficiently compressed to have a high pressure and temperature. Therefore, the specific heat of the mixture is large, causing low pressure rise rate with same amount of heat. As shown in figure 24, the amount of heat from gas to wall was slightly higher at B/S ratio of 1.0, mainly attributed to the larger diameter of piston (i.e. bore size). However,

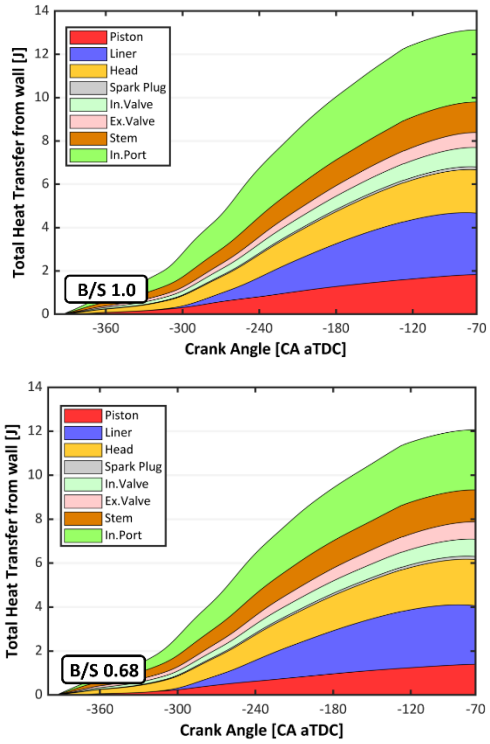

Figure 23. Total heat transfer amount from the walls to gas at 2000 rpm during intake stroke; top: B/S ratio of 1.0; bottom: B/S ratio of 0.68

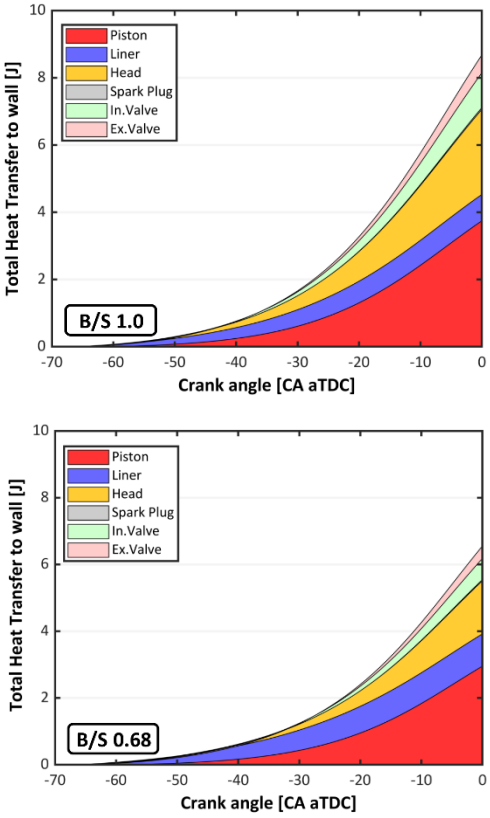

Figure 24. Total heat transfer amount from the gas to walls at 2000 rpm during compression stroke; top: B/S ratio of 1.0; bottom: B/S ratio of 0.68

due to the higher specific heat, the effect on decrements of pressure and temperature was small.

Regarding these results, both the temperature and pressure of B/S ratio of 1.0 were higher than those of B/S ratio of 0.68, which were negative effects with respect to the knock-resistive behavior. Nonetheless, these impacts only variated less than 10K differences of the gas temperature near the ignition timing. In addition, it was observed that there was no remarkable advantage of increase in heat transfer during compression stroke (after the inverse timing) for further knock suppression in B/S ratio of 0.68 due to its smaller surface areas. In conclusion, in lower B/S ratio, it is thought that KLSA advance and increase in efficiency were achieved by increased flame speed and short flame travel distance during the combustion.

The increase in efficiency of decreasing B/S ratio below 0.83 shows no remarkable change, whereas low B/S ratio generally increases additional friction loss and has a disadvantage of packaging for engine design. In addition, as it was observed in the part load conditions, efficiency increase during decreasing B/S ratio was saturated at near B/S ratio of 0.83. Therefore, to investigate the origin of increased heat transfer in lower B/S ratio, a further investigation in heat loss during combustion is necessary. As the lower B/S ratio engine has the larger surface area of cold cylinder liner wall, it may affect to the deterioration of efficiency, especially from the late combustion phase until the exhaust valve opening. From the results, the proper cooling strategies may be suggested.

Conclusions

In this study, the effects of the bore-to-stroke ratio on efficiency and knock characteristics were investigated using a single-cylinder GDI engine with experiments and simulations. Three bore-to-stroke ratios, 1.0, 0.83, and 0.68, with a constant displacement volume (0.5 L) and compression ratio (12) were tested at 1500 and 2000 rpm.

1. In the constant part load condition (4.5, 6.5 bar of nIMEP), due to the higher cooling loss and exhaust loss under a B/S ratio of 0.68 (compared to other B/S ratios), it was shown that the indicated efficiency was not monotonically increased as the B/S decreased below 0.83 in both 1500 and 200rpm cases. It was originally expected that cooling loss would be decreased at lower B/S ratios; however, the possibility of increased heat transfer was noticed.

2. In part load condition, higher B/S ratio showed an advantage of initial flame growth and speed. It was observed as retarded spark timing, and using 3D simulation, it was found that mixture velocities were faster than other B/S ratios of 0.83 and 0.68 near the spark plug. Lower B/S ratio engine showed a disadvantage of the formation of tumble motion due to its geometrical reason. In addition, decreasing B/S ratio below 0.83 showed no additional increase in turbulent intensity, and it was also observed in the experiment as the sufficiently short burn durations in B/S 0.83 case.

3. Under knocking combustion, through an experiment with a constant fuel input (26 mg/cycle), an attempt was made to equalize the initial condition of the engine cycle. As a result, at KLSA condition in 1500 rpm case, B/S ratios of 0.83 and 0.68 showed no significant difference in burn duration. However, B/S ratio of 0.68 showed the highest efficiency. In this condition, it was thought that the heat transfer loss was decreased as the S/V ratio was reduced.

4. At a relatively high engine speed (2000 rpm), the highest efficiency was achieved at the lowest B/S ratio of 0.68 due to the most advanced KLSA. However, the advantage was not remarkable and the B/S ratio of 0.83 showed its less heat loss amount. While in general, a shorter burn duration has the potential to increase gross work, the experimental results confirmed that the gross work potential is saturated around the B/S 0.83 condition. These results indicate that, over a certain engine speed or B/S condition, the flow enhancement obtained by an additional decrease in B/S may lead to a greater amount of cooling loss. Therefore, it can be suggested that a B/S reduction with constant compression ratio and displacement volume may not lead to monotonic increases in engine efficiency.

5. Based on engine experimental data, a 1D engine model was established and validated both in motoring and firing conditions. It was found that the thermal boundary conditions could be varied by the geometrical differences. As the valve timing was controlled to be maintained consistent in all B/S conditions, the residual gas fraction was not significantly different among the different B/S conditions.

6. Using 3D simulation, the impacts of thermal boundary temperatures on fresh mixture was investigated at KLSA knocking conditions. Lower B/S ratios showed the less heat transfer despite the higher surface temperatures, which contributed to a lower unburned gas temperature at IVC timing. However, it was found that there's no significant advantage in decreasing the gas temperature by heat transfer during the compression stroke in lower B/S ratio due to the reduced surface area. It is thought that higher knock resistance in lower B/S ratio was originated from shorter flame travel distance, therefore, a further investigation on combustion process is still necessary.

References

1. European Commission. "Proposal for post-2020 CO2 targets for cars and vans." European Commission, 2018, accessed 9-Oct-2018, 2018, https://ec.europa.eu/clima/policies/transport/vehicles/proposal_en.
2. Vuilleumier, D. and Sjöberg, M., "Significance of RON, MON, and LTHR for Knock Limits of Compositionally Dissimilar Gasoline Fuels in a DISI Engine." *SAE Int. J. Engines* 10(3):938-50, 2017, doi:10.4271/2017-01-0662.
3. Kim, N., Kim, J., Ko, I., Choi, H. et al. "A Study on the Refinement of Turbulence Intensity Prediction for the Estimation of In-Cylinder Pressure in a Spark-Ignited Engine." SAE International, 2017, doi:10.4271/2017-01-0525.
4. Kolodziej, C. P., Pamminger, M., Sevik, J., Wallner, T. et al. "Effects of Fuel Laminar Flame Speed Compared to Engine Tumble Ratio, Ignition Energy, and Injection Strategy on Lean and EGR Dilute Spark Ignition Combustion." *SAE Int. J. Fuels Lubr.* 10(1):82-94, 2017, doi:10.4271/2017-01-0671.
5. Anderson, M. K., Assanis, D. N., and Filipi, Z. "First and Second Law Analyses of a Naturally-Aspirated, Miller

Cycle, SI Engine with Late Intake Valve Closure." SAE International, 1998, doi:10.4271/980889.
6. Poulos, S. G. and Heywood, J. B. "The Effect of Chamber Geometry on Spark-Ignition Engine Combustion." SAE International, 1983, doi:10.4271/830334.
7. Bianchi, G. M., Cantore, G., Mattarelli, E., Guerrini, G. et al. "The Influence of Stroke-to-Bore Ratio and Combustion Chamber Design on Formula One Engines Performance." SAE International, 1998, doi:10.4271/980126.
8. Filipi, Z. S. and Assanis, D. N., "The effect of the stroke-to-bore ratio on combustion, heat transfer and efficiency of a homogeneous charge spark ignition engine of given displacement." *International Journal of Engine Research* 1(2):191-208, 2000, doi:10.1243/1468087001545137.
9. Ikeya, K., Takazawa, M., Yamada, T., Park, S. et al. "Thermal Efficiency Enhancement of a Gasoline Engine." *SAE Int. J. Engines* 8(4):1579-86, 2015, doi:10.4271/2015-01-1263.
10. Nakata, K., Nogawa, S., Takahashi, D., Yoshihara, Y. et al. "Engine Technologies for Achieving 45% Thermal Efficiency of S.I. Engine." *SAE Int. J. Engines* 9(1):179-92, 2015, doi:10.4271/2015-01-1896.
11. Severi, E., d'Adamo, A., Berni, F., Breda, S. et al. "Numerical investigation on the effects of bore reduction in a high performance turbocharged GDI engine. 3D investigation of knock tendency." *Energy Procedia* 81:846-55, 2015, doi:10.1016/j.egypro.2015.12.094.
12. Hoag, K. L., Mangold, B., Alger, T., Abidin, Z. et al. "A Study Isolating the Effect of Bore-to-Stroke Ratio on Gasoline Engine Combustion Chamber Development." *SAE Int. J. Engines* 9(4):2022-29, 2016, doi:10.4271/2016-01-2177.
13. Cho, S., Song, C., Oh, S., Min, K. et al. "An Experimental Study on the Knock Mitigation Effect of Coolant and Thermal Boundary Temperatures in Spark Ignited Engines." SAE International, 2018, doi:10.4271/2018-01-0213.
14. Oh, S., Cho, S., Seol, E., Song, C. et al. "An Experimental Study on the Effect of Stroke-to-Bore Ratio of Atkinson DISI Engines with Variable Valve Timing." SAE International, 2018, doi:10.4271/2018-01-1419.
15. Ayala, F. A., Gerty, M. D., and Heywood, J. B. "Effects of Combustion Phasing, Relative Air-fuel Ratio, Compression Ratio, and Load on SI Engine Efficiency." SAE International, 2006, doi:10.4271/2006-01-0229.
16. Gaeta, A., Giglio, V., Police, G., and Rispoli, N. J. F., "Modeling of in-cylinder pressure oscillations under knocking conditions: A general approach based on the damped wave equation." *Fuel* 104:230-43, 2013, doi:10.1016/j.fuel.2012.07.066.
17. Draper, C. S., "Pressure waves accompanying detonation in the internal combustion engine." *Journal of the Aeronautical Sciences* 5(6):219-26, 1938, doi:10.2514/8.590.
18. Cho, S. "Study on the Efffect of Cylinder Wall Temperatures on Knock Characteristics in Spark-Ignited Engine." Ph.D Dissertation, Dept. Mechanican and Aerospace Engineering, Seoul National University, Seoul, South Korea, 2018.
19. Song, H., Padmanabhan, A., Kaahaaina, N., and Edwards, C., "Experimental study of recompression reaction for low-load operation in direct-injection homogeneous charge compression ignition engines with n-heptane and i-octane fuels." *International Journal of Engine Research* 10(4):215-29, 2009, doi:10.1243/14680874JER03309.
20. Imaoka, Y., Shouji, K., Inoue, T., and Noda, T., "A Study of Combustion Technology for a High Compression Ratio Engine: The Influence of Combustion Chamber Wall Temperature on Knocking." *SAE Int. J. Engines* 9(2):768-76, 2016, doi:10.4271/2016-01-0703.
21. Inoue, Y., Morioka, R., Sato, K., Higashi, H. et al. "Effects of heat transfer in intake ports on engine performance." JSAE 20185297, JSAE, 2018.
22. Uozumi, H., Kawamura, Y., Matsuki, H., Ikeda, T. et al. "Low-heat-transfer Combustion Chamber for Improvement of Knocking." JSAE 20185348, JSAE, 2018.

Contact Information

Seokwon Cho, PhD,
Dept. Mechanical and Aerospace Engineering, Seoul National University
seokwon@snu.ac.kr

Sechul Oh
Dept. Mechanical and Aerospace Engineering, Seoul National University
sc150@snu.ac.kr

Han Ho Song, PhD, Associate Professor,
Dept. Mechanical and Aerospace Engineering, Seoul National University
hhsong@snu.ac.kr

Kyoungdoug Min*, PhD, Professor,
Dept. Mechanical and Aerospace Engineering, Seoul National University
kdmin@snu.ac.kr

Acknowledgments

This work was comprised of results from the industrial-educational cooperation project (0420-20160109, "Investigation on the effect of stroke-to-bore ratio on gasoline engines with simulations and experiments") of Hyundai Motor Company, Hyundai NGV and Seoul National University. The test facility was supported by Advanced Automotive Research Center (AARC) and Institute of Advanced Machinery and Design (IAMD) of Seoul National University. The authors would like to express our sincere gratitude to their support.

Definitions/Abbreviations

1D	one-dimensional
3D	three-dimensional
aBDC	after bottom dead center
aTDC	after top dead center
B/S	bore-to-stroke
bBDC	before bottom dead center
BDC	bottom dead center

bTDC	before top dead center
CA	crank angle
CA10	crank angle at burned mass fraction of 10%
CA50	crank angle at burned mass fraction of 50%
CA90	crank angle at burned mass fraction of 90%
CFD	computational fluid dynamics
CO2	carbon dioxide
CVVT	continuous variable valve timing
DoE	design of experiment
EVC	exhaust valve closing
EVO	exhaust valve opening
GDI	gasoline direct injection
H/C	hydrogen-to-carbon
IMEP	indicated mean effective pressure
ISFC	indicated specific fuel consumption
ITE	indicated thermal efficiency
IVC	intake valve closing
IVO	intake valve opening
KLSA	knock limit spark advance
LHV	low heating value
LIVC	late intake valve closing
MAPO	maximum amplitude of pressure oscillation
MBT	maximum brake torque
nIMEP	net indicated mean effective pressure
nISFC	net indicated specific fuel consumption
nITE	net indicated thermal efficiency
NOx	nitrogen oxides
RGF	residual gas fraction
S/V	surface-to-volume
SI	spark-ignited
SOC	start of combustion
SSE	sum of squared error
TDC	top dead center